SIMULTANEOUS ACCELERATION OF TWO IONS WITH UNEQUAL MASS-TO-CHARGE RATIO IN A SYNCHROTRON

D. Ondreka*, H. Liebermann, A. Pastushenko, P. Spiller
GSI Helmholtz Centre for Heavy Ion Research, Darmstadt, Germany
E. Renner, TU Wien, Vienna, Austria

Abstract

In this contribution, we report on the successful simultaneous acceleration of a beam composed of two different ions with unequal mass-to-charge ratio within the same cycle of the heavy ion synchrotron SIS18 at GSI. While acceleration of multiple charge states of a single ion species has been accomplished in linear accelerators, in a synchrotron this has never been done before to the knowledge of the authors. In a proof-of-principle experiment, low intensities of $^{56}Fe^{25+}$ and $^{209}Bi^{68+}$ were successively injected with horizontal multi-turn injection. Using two RF cavities, each ion species was then independently captured and accelerated in the same magnetic fields at its respective revolution frequency, the bunches of the lighter ion continuously overtaking those of the heavier ion. Such a beam composed of different ions has potential applications in particle therapy, plasma physics, nuclear physics, and materials research. The distinct revolution frequencies make this scheme attractive whenever independent control over the extraction of both ions is desired.

INTRODUCTION

Accelerators are usually designed to deliver one ion species at a time. For many applications, this is sufficient, since fast switching of ion species can be implemented if necessary. However, there are applications where simultaneous acceleration of different ion species is very useful. We focus here on cases where the difference in mass-to-charge ratio prevents simultaneous acceleration when setting up the accelerator for a single ion. For brevity, we denote this scenario *multi-species acceleration* in this contribution.

In linear accelerators, acceleration of several charge states of one isotope has been successfully demonstrated at FRIB [1, 2] and at GSI [3]. There, the goal is to increase beam intensity by reducing losses due to the broad charge state distribution of heavy ions after a stripping stage. In a synchrotron, multi-species acceleration has never been achieved before to the knowledge of the authors. Demonstrating the feasibility is therefore interesting in itself. In addition, there are real applications that would profit from simultaneous delivery of two ion species. For instance, in plasma physics experiments a heavy ion for target heating could be accompanied by a light ion serving to probe the generated plasma. In fact, this idea was brought up at GSI more than two decades ago [4], but not realized at the time.

* d.ondreka@gsi.de

Recently, the idea got attention in relation to developments of the GSI biophysics group for online range monitoring in particle therapy (PT) [5]. This concept requires, in addition to the main ion used for treatment (usually carbon), simultaneous delivery of a lighter ion with sufficient range to traverse the patient. While a mixture of ^{12}C and ^{4}He can be provided by single-species acceleration [6, 7], dual-species acceleration would allow for more ion combinations and provide additional flexibility through independent control of the two spills using KO extraction in this context.

SIS18 with its injector UNILAC satisfies all prerequisites for dual-species acceleration. It supports fast switching of ion species and has enough RF cavities to enable two independent RF programs. With the advent of the FAIR control system (FAIR-CS) [8], developed over the last years to support complex operation modes of SIS18 and the two storage rings ESR and CRYRING, the implementation of this scheme became possible. We therefore took an experimental approach and programmed the necessary extensions for incorporating a second ion species and and additional RF program into the SIS18 machine model. The scheme was tested when the beam time schedule offered $^{56}Fe^{25+}$ and $^{209}Bi^{68+}$ at once. This combination is by chance similar to $^{3}He^{2+}$ and $^{12}C^{6+}$, which constitutes an attractive choice for online range monitoring in PT.

IMPLEMENTATION

The two ions to be accelerated in SIS18 are characterized by their mass-to-charge ratios $(m/q)_1 < (m/q)_2$. Since UNILAC delivers either ion with the same energy of 11.3 MeV/u, ion 1 is injected first and accelerated to the magnetic rigidity for injection of ion 2. Next, ion 2 is injected and both ion species are accelerated with the same field ramp, each having its own RF program. As SIS18 employs multi-turn injection, horizontal phase space must be shared between the two ions. This requires the amplitude of the time-dependent bump at the injection septum to be reduced for the second injection, much like in the scheme used to create mixed $^{12}C/^{4}He$-beams for research in PT at MedAustron [9].

When implementing this concept, we were able to build on the unified modular settings management system for all circular accelerators integrated into the FAIR-CS. This system has been developed at GSI based on the LSA framework [10, 11] in a collaboration between machine physicists and control system experts. Essentially, it enables machine physicists to program new operation modes by creating new cycle types

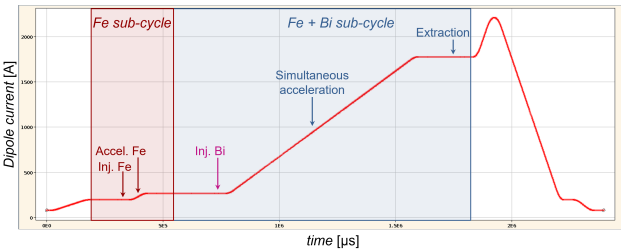

Figure 1: Cycle for dual-species acceleration. The curve represents the current in the main bending magnets.

and by adapting the hierarchy of parameters representing the machine along with the rules for calculating set values.

For dual-species acceleration, the cycle was composed of *sub-cycles*, a concept originally invented to structure storage ring cycles. Employing sub-cycles was essential to accomodate the ion-dependent set values for the injection devices and to communicate the requested ion species to the UNILAC. The two sub-cycles for beam manipulation each contain one injection and an acceleration ramp, as can be seen in Fig. 1. Moreover, the hierarchy for SIS18 was extended by adding parameters for a second ion and a second set of RF parameters (see Fig. 2). The magnetic cycle is calculated based on ion 1, which is present over the whole cycle. RF parameters are then calculated for each ion using the same algorithms with corresponding input parameters. The correct execution of the RF program for the second beam required only one small manual intervention in the low-level RF system to switch of synchronization of the cavity for ion 2 with the master DDS, which does not yet support a second RF program. The cycle was tested without beam before the actual experiment to verify the consistency of set values and timing. This proved crucial since several errors were found that would have prevented execution of the experiment.

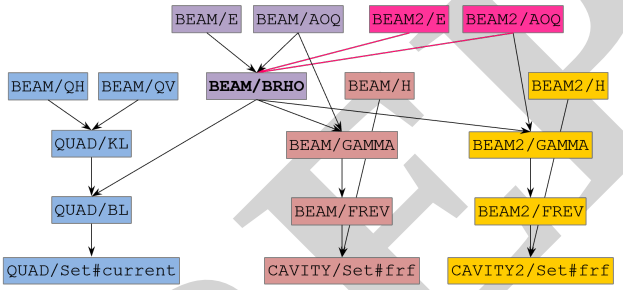

Figure 2: Parameter hierarchy for dual-species acceleration (schematic), extended by parameters for the second ion (red) and a second RF program (yellow).

The choice of RF harmonics was determined by the requirement that the RF frequency $h_2 f_2$ of ion 2 must not be a harmonic of the revolution frequency f_1 of ion 1 to avoid distortions of the RF bucket of ion 1. As $f_1(t)$ and $f_2(t)$ are given, we must select h_2 such that $h_2 f_2(t)/f_1(t)$ never equals an integer. For ion 2 a analogous relation applies. These relations clearly favor lower harmonics and stipulated the use of two broad-band MA cavities with $h_1 = h_2 = 2$ instead of the ferrite cavities with $h = 4$.

EXPERIMENTAL RESULTS

The results presented here are based on data obtained during a single session lasting four hours, focused on demonstrating feasibility of dual-species acceleration with Fe (ion 1) and Bi (ion 2). Our main observable was beam current measured with a DC current transformer (DCT), stored for offline analysis. No other instrumentation was recorded because we had not planned for systematic investigations due to the limited time available.

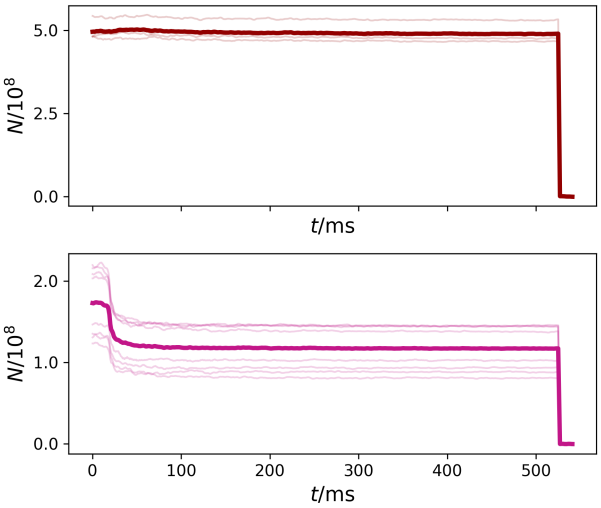

Figure 3: Intensity of Fe (top) and Bi (bottom) in the second sub-cyle after optimization with single RF and nominal injection bump amplitude. The zero of time is at the start of RF capture. The thick dark lines correspond to the average of the thinner traces, which are data for individual cycles.

Both beams were first set up individually in single-species mode without the RF for the other ion and with nominal amplitude of the injection bump (85 mm). Optimization of injection and acceleration was only done up to a point where reasonable intensities and efficiencies were reached to save time. For Fe, produced in a Penning ion source, the injector current was generally very stable, with average values ranging from 60 µA to 80 µA and pulse-to-pulse variations with a standard deviation of 8 µA. After injection optimization, 7 turns were effectively stored in SIS18 with an injected pulse length of 80 µs, corresponding to an acceptable injection efficiency of about 41%. Acceleration efficiency was 85% over the whole cycle, which is comparable to standard cycles. RF voltage was determined by setting a reference momentum spread of $\sigma_\delta = 5 \cdot 10^{-4}$. Under these conditions, the number of particles on flattop was $5 \cdot 10^8$. The injector current of Bi had larger pulse-to-pulse fluctuations, which is typical for a beam created in the high-current ion source (VARIS). During the first half of the experiment, average current varied between 40 µA and 80 µA at a standard deviation of 22 µA for pulse-to-pulse variations. Later, current was raised to 100 µA (std. dev. 10 µA) to compensate for the observed high losses when operating with both beams. After injection optimization, 8.5 turns were stored in SIS18

at a pulse length of 80 µs, corresponding to an injection efficiency of 50%. Acceleration efficiency was 67%, with RF voltage again defined by a reference momentum spread of $\sigma_\delta = 5 \cdot 10^{-4}$. The lower acceleration efficiency can be explained by a larger momentum spread of the Bi-beam from the injector compared to Fe. Under these conditions, the number of particles on flattop was $1 - 1.5 \cdot 10^8$. Figure 3 shows intensity versus time in the second sub-cycle for both beams after the individual optimization.

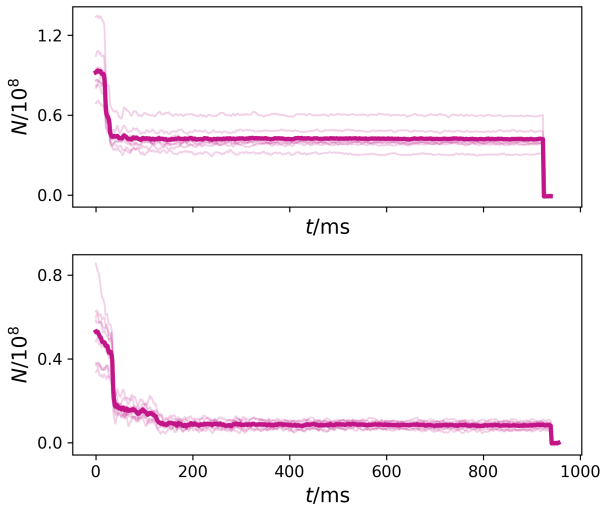

Figure 4: Intensity of Bi with Fe-RF on. Top and bottom trace correspond to injections with 85 mm and 42 mm bump amplitude. The lower initial value for 85 mm bump compared to Fig. 3 is mostly due to lower injector current (40 µA vs. 60 µA), but a change of Q_x from 4.28 to 4.3 adds to it. The step at 120 ms in the bottom trace is probably a result of keeping the injection pulse length unchanged.

After setup of the individual beams, the experiment was continued with Bi, but now with the RF for the Fe-beam switched on. Initially, the Bi-beam was almost lost completely at the start of the ramp. Since this came unexpected, many knobs were tried to reduce losses. A larger amplitude of the injection bump lead to better transmission to flattop, indicating that particles with larger horizontal emittance get lost predominantly. However, the maximum bump amplitude for Bi had to be limited to leave room for the Fe-beam. Transverse tunes also influenced losses, but the final working point $(Q_x, Qy) = (4.3, 3.28)$ was only marginally different from the initial one $(4.295, 3.27)$. In fact, losses depended most strongly on the amplitude of the RF voltage of the Fe-beam, which was found out by manually scaling this voltage down. To prepare for dual-species acceleration, it was then decided to reduce both the ramp rate from 2 T/s to 1 T/s and the reference momentum spread for the RF voltage from $\sigma_\delta = 5 \cdot 10^{-4}$ to $\sigma_\delta = 3 \cdot 10^{-4}$. As a result, peak RF voltages dropped from 9.6 kV to 4.4 kV for Bi and from 8.7 kV to 4.0 kV for Fe. While the reduced bucket area slightly increased capture losses, overall survival of the Bi-beam was much better. Figure 4 displays intensity of the Bi-beam under the influence of the Fe-RF, both with nominal amplitude of the injection bump and with amplitude reduced for dual-species operation (42 mm). Note that those intensities cannot be directly compared to the ones reached during setup due to changes in injector current and working point between measurements. However, the Bi-beam is obviously strongly affected by the Fe-RF.

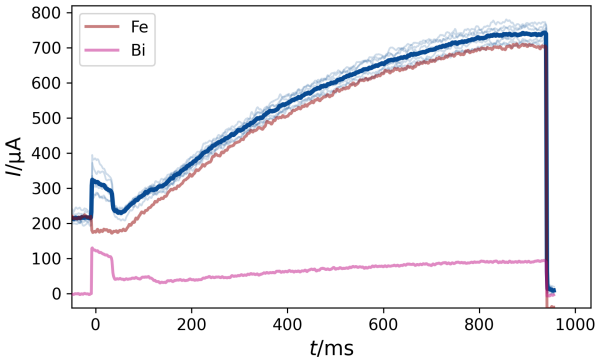

Figure 5: Beam current for acceleration of Fe and Bi. Thin blue traces correspond to individual cycles, the thick blue trace marking their average. For comparison, average traces for Fe (brown) and Bi (pink) in individual operation with both RF cavities on are shown. The current offsets at the end of the cycle are artifacts.

When injection of Fe was activated again, the DCT measurements indicated simultaneous acceleration. Figure 5 shows the current traces in dual-species operation, compared to averaged current traces for single-species operation. The Bi-trace was definitely acquired with both RF systems on, whereas for Fe this is very likely but not entirely certain due to missing data on the status of the RF systems. The single-species traces were rescaled to match the respective injected currents. Qualitatively, one can deduce from this comparison that losses of the Fe-beam cannot have been very large in dual-species operation. A quantitative comparison is, however, not possible due to baseline fluctuations in the current traces caused by an unfortunate choice of gain. Therefore, we are presently not able to tell whether the Bi-RF caused losses in the Fe-beam and whether interactions between the beams created additional losses. To answer these questions, additional experiments under more controlled conditions are necessary. Table 1 summarizes the most important machine and beam parameters for the demonstration experiment.

Table 1: Machine and Beam Parameters

	$^{56}Fe^{25+}$	$^{209}Bi^{68+}$
Working point (h, v)	4.3, 3.28	
Acceptance (h, v)	150 µm, 50 µm	
Ramping speed	1 T/s	
Injection energy	11.36 MeV/u	11.14 MeV/u
Extraction energy	673.4 MeV/u	400.0 MeV/u
Injection bump	85 mm	42 mm
Max. RF voltage	4.0 kV	4.4 kV
Intensity (injected)	$2 \cdot 10^8$	$6 \cdot 10^7$

Since the current traces were difficult to interpret during the experiment, we decided to prove that there is simultaneous acceleration by separating the two beams horizontally and make them appear in different positions on a scintillating screen behind the magnetic extraction septum after fast extraction. To this end, the RF frequencies of both beams were shifted on flattop in opposite directions to create momentum deviations of $\delta = -5 \cdot 10^{-3}$ for Fe and $\delta = 7.5 \cdot 10^{-3}$ for Bi. To fit both beam spots on the screen, beam size was limited by reducing the injection pulses to 20 µs for Fe and 5 µs for Bi, while increasing the injection bump amplitude to 50 mm for the latter. This also helped in avoiding saturation of the screen, which is very sensitive especially for ions with a high atomic number like Bi. The result is diplayed in Fig. 6.

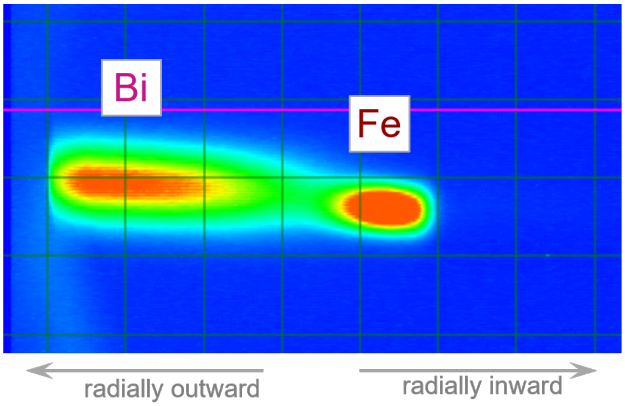

Figure 6: Radially separated spots of both beams on a scintillating screen behind the magnetic extraction septum. The larger horizontal spot size of Bi corresponds to its larger emittance due to the double-injection scheme.

SIMULATIONS

The high losses in the Bi-beam under the influence of the RF voltage for the Fe-beam would certainly limit the usability of this scheme for practical applications. On the other hand, the experimental data did not give a direct hint at the physical origin of the losses. We therefore set out to better understand dual-species acceleration theoretically. It was, however, not quite clear how to simulate this scheme.

We decided to first implement a simple time-based longitudinal tracking, in which the two cavities are represented by their voltage programs $U_i(t) = \hat{U}_i(t) \sin(\phi_i(t))$, with the phase $\phi_i(t)$ derived by integrating the relativistic $\beta_i(t)$ as a function of the momentum ramp $\beta_i\gamma_i(t)$ of the respective beam. Each particle then receives an energy kick at the cavity according to its absolute arrival time. The revolution time is calculated from actual velocity and path length, which includes the contribution of momentum-compaction to first order. Momentum deviation is obtained by subtracting the reference momentum defined by the acceleration ramp from the actual momentum. When applied with only the RF voltage for the respective ion species, this tracking reproduces the correct momentum gain and yields the expected behavior in longitudinal phase space. Adding the RF voltage for the second ion species results in a small high-frequency modulation of the longitudinal phase space coordinates on top of the slow variations at the synchrotron frequency, but otherwise does not lead to emittance blow-up. At the same time, the tracking shows a strong influence up to the point of particle loss, if the second RF frequency becomes a multiple of the revolution frequency of the first ion, as expected by the considerations on the choice of harmonics. Having validated our tracking this way, we concluded that the high losses observed in the Bi-beam are most likely not caused by longitudinal emittance blow-up.

It was thus clear that we needed to include transverse dynamics in the simulations. We therefore went on to implement 6-D-tracking for dual-species acceleration using Xsuite [12]. Unlike our longitudinal time-based tool, Xsuite performs tracking on a turn-by-turn basis. It is therefore presently not possible to parametrize the two RF cavity elements by the absolute phases $\phi_i(t)$ as above. Instead, we first decide on the ion species to be simulated, for which we use the index 1. The cavity element C_1 for ion 1 is parametrized by its RF harmonic h_1, with the phase being implicitly defined by the arrival time of the reference particle. The cavity element C_2 for ion 2 is parametrized by its frequency and lag parameters, which are both made time-dependent. The frequency parameter is set to the RF frequency program $f_{\mathrm{RF},2}(t) = h_2 f_2(t)$ for ion 2, while the lag parameter is set to the phase difference $\phi_2(t) - \phi_1(t)$. The RF voltage amplitude program $\hat{U}_i(t)$ of either cavity is defined by means of the voltage parameter. Finally, the momentum ramp for ion 1 is specified as energy program. With this set-up, we can use Xsuite to simulate the effect of cavity C_2 on ion 1. There seems to be presently no way to simulate both beams at the same time in Xsuite due to the implicit definition of time in terms of the reference particle (ion 1), which differs from that of ion 2. However, as long as we neglect interactions between the two beams, this is actually not necessary.

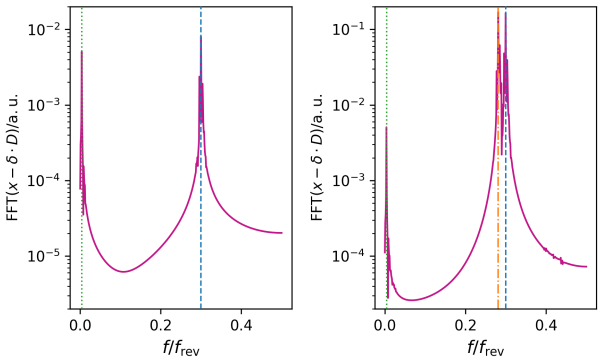

Figure 7: Frequency spectra of $x - \delta \cdot D_m$ for a single Bi particle without (left) and with (right) Fe-RF. The peaks corresponding to horizontal and synchrotron tunes are marked with blue dashed and green dotted lines, respectively. The peak corresponding to the modulation frequency by the Fe-RF in the right plot is indicated by an orange dashdotted line. Notice the different scales of the two plots.

The first simulations for Bi were done with a small number of particles for a stationary bunched beam at injection level. Inspection of the turn-by-turn data revealed that the Fe-RF leads to a large horizontal oscillation at the RF frequency $f_{\mathrm{RF,Fe}}$. The necessary coupling from longitudinal to horizontal motion is provided by dispersion, which is non-zero everywhere in SIS18, having values $D_{\mathrm{Bi}} = 1.6\,\mathrm{m}$ at the cavity for Bi and $D_{\mathrm{Fe}} = 2.1\,\mathrm{m}$ at the cavity for Fe. Figure 7 shows the frequency spectra of the residual $\Delta x_k = x_k - \delta_k \cdot D_m$, obtained by tracking a single Bi particle over 1024 turns and sampling the coordinates for each turn k at the location of a monitor m, where D_m is the dispersion at the monitor, both without and with the Fe-RF. The particle was started on the design orbit with reference momentum, but with a phase offset from the bucket center. Therefore, the energy kicks at the cavity excite small horizontal betatron oscillations whose amplitude increases and decreases at the synchrotron frequency. This is reflected by the peak at the horizontal betatron frequency of 0.3. When the Fe-RF is on, the betatron oscillation amplitudes are much stronger, and a second peak appears corresponding to a modulation of the horizontal position at the frequency of the Fe-RF. Counting time in turns, the modulation frequency is given by $f_{\mathrm{RF,Fe}}/f_{\mathrm{Bi}} \mod 1$, mirrored into the interval $[0, 0.5]$ through aliasing.

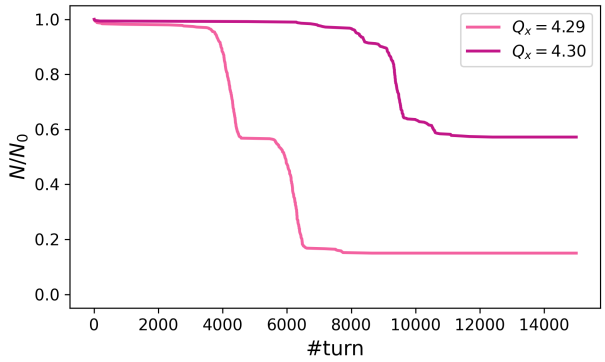

Figure 8: Bi intensity vs. turn from the tracking simulations. Losses shift to later times with increasing Q_x.

This modulation at the frequency of the Fe-RF does not lead to a growth of horizontal emittance, as long as the modulation frequency does not coincide with a horizontal betatron sideband. Indeed, no emittance growth was observed under the above conditions even when tracking over tens of thousands of turns. However, since frequencies change during the acceleration ramp, the modulation frequency for Bi rises quickly from its initial value of 0.28, crossing the fractional horizontal tune 0.3 within the first 60 ms of the ramp. To verify if losses in the Bi-beam are observed in simulations and related to horizontal tune, we performed multi-particle simulations over the first 15000 turns (or 58 ms) of the acceleration ramp, using a simplified RF program with constant voltage. The initial distribution contained 500 particles with realistic geometric RMS-emittances of 25 µm (hor.) and 5 µm (vert.). Total bunch length was set to about 20 % of the RF period for an RF voltage of 7.8 kV. Results of simulations for Q_x equal to 4.29 and 4.3 are shown in Fig. 8, where the shift of losses to later times with increasing tune is clearly visible. Qualitatively, the data can be compared to the top plot of Fig. 4, as horizontal phase space was filled in the simulations. However, for a quantitative comparison, the simulations have to be extended to include the real RF program and the change of lattice functions during the acceleration ramp. This will be the subject of further studies.

In contrast, the modulation frequency for the Fe-beam caused by the Bi-RF stays well above 0.3 for 90 % of the cycle. When it finally crosses the horizontal tune, we indeed observe a growth of horizontal emittance by 50 % in simulations, but adiabatic damping probably prevents significant losses. In future experiments, we intend to measure the corresponding emittance growth.

CONCLUSION

We demonstrated simultaneous acceleration of the two ions $^{56}Fe^{25+}$ and $^{209}Bi^{68+}$ with unequal mass-to-charge ratio in SIS18, which to the knowledge of the authors has never before been achieved in a synchroton. In this proof-of-principle experiment, high losses were observed in the Bi-beam under the influence of the RF for the Fe-beam, while the Fe-beam was much less affected by the RF for the Bi-beam. Quantitative statements on losses of the Fe-beam and on the possible influence of the second beam cannot be made with the available data. These topics require dedicated experiments under more controlled conditions.

To understand the origin of the observed losses, simulation schemes for dual-species acceleration have been developed. First results from longitudinal simulations appear to rule out longitudinal emittance blow-up as a cause. Tracking simulations with Xsuite indicate that losses are a consequence of horizontal emittance blow-up mediated by non-zero dispersion at the cavity, whenever the RF frequency of the other ion coincides with a horizontal betatron sideband. Again, a quantitative comparison requires refined simulations and additional experimental data.

However, we are confident to have identified the major cause of the observed losses. In SIS18, exication of the Bi-beam would be avoided by choosing a different horizontal tune, e.g. $Q_x = 4.15$ as used in high-current operation. Also, losses are generally expected to be strongly suppressed if dispersion at the cavity is zero. As this option does not exist in SIS18, we intend to test the scheme at other machines in the near future.

ACKNOWLEDGEMENTS

We thank the GSI ring RF group for their support in performing the experiment. Also, we are indebted to H. Bräuning from the GSI BI group for help with correction of artifacts in the DCT measurements. Finally, we are grateful to G. Iadarola (CERN) and K. Holzfeind (TU Wien) for their advice on using Xsuite for simulating the effect of the cavity for a second ion species.

REFERENCES

[1] P. N. Ostroumov *et al.*, "Simultaneous acceleration of multiply charged ions through a superconducting linac", *Phys. Rev. Lett.*, vol. 86, no. 13, p. 2798, 2001. doi:10.1103/PhysRevLett.86.2798

[2] P. N. Ostroumov *et al.*, "First simultaneous acceleration of multiple charge states of heavy ion beams in a large-scale superconducting linear accelerator", *Phys. Rev. Lett.*, vol. 126, no. 11, p. 114801, 2021. doi:10.1103/PhysRevLett.126.114801

[3] W. Barth *et al.*, "High performance megawatt uranium beams at GSI UNILAC", in *Proc. LINAC'24*, Chicago, IL, USA, Aug. 2024, pp. 400–403. doi:10.18429/JACoW-LINAC2024-TUPB030

[4] I. Hofmann *et al.*, "In-flight imaging of heavy ion driven plasma targets", in *GSI-Report GSI-2001-4*, GSI, Darmstadt, pp. 29f, Oct. 2001.

[5] L. Volz *et al.*, "Experimental exploration of a mixed helium/carbon beam for online treatment monitoring in carbon ion beam therapy", *Phys. Med. Biol.*, vol. 65, no. 5, p. 055002, 2020. doi:10.1088/1361-6560/ab6e52

[6] E. Renner *et al.*, "First mixed He/C ion beams at a clinical facility: Two years from concept to first ion imaging experiment", presented at IPAC'26, Deauville, France, May 2026, paper TUO8T01, this conference.

[7] A. Pastushenko *et al.*, "Flat C/He spills for online range monitoring in particle therapy", presented at IPAC'26, Deauville, France, May 2026, paper THP4093, this conference.

[8] A. Schaller *et al.*, "Storage Ring Mode for FAIR", in *Proc. PCaPAC'22*, Prague, Czech Republic, Feb. 2023, pp. 34–36. doi:10.18429/JACoW-PCaPAC2022-THPP3

[9] M. Kausel *et al.*, "Double multiturn injection scheme for generating mixed helium and carbon ion beams at medical synchrotron facilities", *Phys. Rev. Accel. Beams*, vol. 28, no. 11, p. 111001, 2025. doi:10.1103/t3b5-1xb6

[10] D. Jacquet, R. Gorbonosov, and G. Kruk, "LSA - the High Level Application Software of the LHC - and Its Performance During the First Three Years of Operation", in *Proc. ICALEPCS'13*, San Francisco, CA, USA, Oct. 2013, pp. 1201–1204.

[11] J. Fitzek, A. Schaller, H. Hüther, and R. Mueller, "Supporting injector operation with the FAIR settings management system", in *Proc. ICALEPCS'25*, Chicago, IL, USA, Sep. 2025, pp. 576–582. doi:10.18429/JACoW-ICALEPCS2025-TUPD023

[12] G. Iadarola *et al.*, "Xsuite: An Integrated Beam Physics Simulation Framework", in *Proc. HB'23*, Geneva, Switzerland, Oct. 2023, pp. 73–80. doi:10.18429/JACoW-HB2023-TUA2I1